Spectral light separator based on deep-subwavelength resonant apertures in a metallic film

Yasin Büyükalp, Peter B. Catrysse,[a] Wonseok Shin, and Shanhui Fan[b]

E. L. Ginzton Laboratory and Department of Electrical Engineering, Stanford University, Stanford, California 94305, USA

We propose to funnel, select, and collect light spectrally by exploiting the unique properties of deep-subwavelength resonant apertures in a metallic film. In our approach, each aperture has an electromagnetic cross section that is much larger than its physical size while the frequency of the collected light is controlled by its height through the Fabry-Pérot resonance mechanism. The electromagnetic crosstalk between apertures remains low despite physical separations in the deep-subwavelength range. The resulting device enables an extremely efficient, subwavelength way to decompose light into its spectral components without the loss of photons and spatial coregistration errors. As a specific example, we show a subwavelength-size structure with three deep-subwavelength slits in a metallic film designed to operate in the mid-wave infrared range between 3 and 5.5 μm. © 2014 AIP Publishing LLC. [http://dx.doi.org/10.1063/1.4887059]

The capability to separate light into its spectral components without loss of photons is of great importance in many optical applications, including spectroscopy and multispectral imaging.[1–3] The detectors in these systems are often large pixel arrays. With the scaling of individual pixels down to the (sub)micron scale, there exists an increasing need to develop such capability with a device at the single-wavelength scale. Conventional optical devices that separate light into its spectral components utilize either prisms or absorbing filters.[1–4] The former are photon efficient, i.e., they do not waste incoming photons, but they are much larger than the wavelength of the light, and do not fit on individual pixels. The latter, on the other hand, can be scaled to the wavelength size, but they are very inefficient since such conventional filtering involves absorption of unwanted spectral components.[1,3,4]

Towards the goal of miniaturizing optical devices that perform spectral separation, a significant number of works have exploited nanophotonic structures.[5–7] Most of these works utilize periodic structures, such as gratings, where the periodicity is comparable to the wavelength of interest. Since one typically needs at least a few periods to achieve spectral separation, it is unlikely that any of these structures has the potential to be miniaturized to the single wavelength scale. As an alternative, Zhang *et al.* recently considered a spectral separation device based on the anti-Hermitian coupling of individual nanoscale resonators.[7] The overall device was at the single-wavelength scale. However, achieving anti-Hermitian coupling requires resonances that overlap and interfere with each other, which as a result limits the spectral selectivity and angular robustness of such a structure as a spectral separating device.

In this paper, we numerically demonstrate a very compact and efficient nanophotonic structure at the subwavelength scale that is capable of decomposing light into its spectral frequency components. For its operation, the device relies on the unique optical properties of deep-subwavelength resonant apertures in metallic films. It is well known that many deep-subwavelength structures, including apertures (e.g., slits,[8,9] circular holes,[10] and rectangular holes[11]), support strong resonances, and therefore, can provide spectral selectivity. It has also been shown that these resonant structures can have electromagnetic cross sections far exceeding their physical size.[12] Here, we show that with proper design, one can pack several of these resonators, each tuned to a slightly different resonance wavelength, in a subwavelength device without causing significant interference between them. Such a device naturally operates as a spectral light separator on a subwavelength scale. Moreover, different resonators collect light at different wavelengths from nearly the same cross-sectional region. This is a very attractive feature for multispectral imaging systems since it minimizes spatial coregistration errors between the different spectral channels.[13]

We now illustrate this subwavelength spectral light separator concept using a structure that consists of three deep-subwavelength slits in a metallic film designed to operate at wavelengths between 3 and 5.5 μm in the mid-wave infrared (MWIR) range (Fig. 1). In our example, the slits are all 30 nm wide and are formed in 1000-, 1250-, and 1500-nm-thick metallic films. The center-to-center separation between adjacent slits is 130 nm. For the MWIR operating range, both the widths of the slits and the separations between them are in the deep-subwavelength range. Without loss of generality, we consider a silver (Ag) film and assume air-filled slits. For comparison, we examine both the cases of lossy and lossless silver.[14]

The interaction of this structure with electromagnetic waves is examined by solving Maxwell's equations using the finite-difference frequency-domain (FDFD) method.[15–19] The FDFD method allows us to directly use tabulated dielectric constants of dispersive materials, such as silver, including both the real and the imaginary parts (for lossless materials, the imaginary parts of dielectric constants are

[a]E-mail: pcatrysse@stanford.edu
[b]E-mail: shanhui@stanford.edu
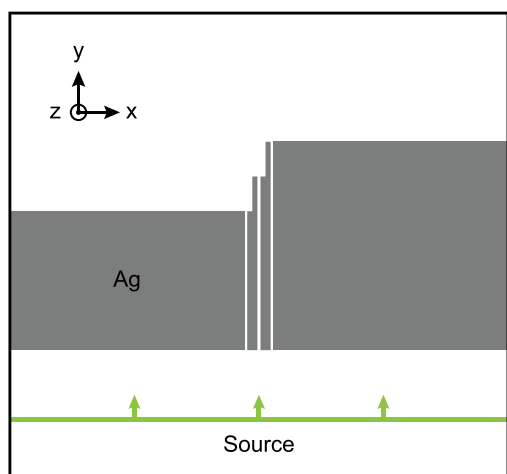
FIG. 1. Geometry of the proposed subwavelength spectral light separator. The device consists of a sequence of three parallel slits in a silver film. The film thickness is different for each slit, but the widths of the slits are the same. The source generates a normally incident plane wave in TM polarization which has only the E_x, E_y, and H_z field components in this coordinate system.

FIG. 2. Transmission cross section spectra of the subwavelength spectral light separator. The solid red lines show the transmission cross section spectra for lossy silver, whereas the dashed blue lines correspond to lossless silver. (a) The individual transmission cross section spectrum for the first slit. (b) The individual transmission cross section spectrum for the second slit. (c) The individual transmission cross section spectrum for the third slit. (d) The overall transmission cross section spectrum for the entire film.

ignored). To simulate a single isolated device, we surround the entire simulation domain by the stretched-coordinate perfectly matched layer (SC-PML), which was proven to produce significantly better frequency-domain solver performance than the more commonly used uniaxial PML.[19]

From the solution of Maxwell's equations, we measure the transmission cross section $\sigma_T(\lambda)$ as a function of wavelength. Here, we are more interested in the transmission cross section of each individual slit rather than the transmission cross section of the entire structure, where the latter is more commonly used in analyzing structures with resonant apertures.[20] To calculate the individual transmission cross section of each slit, we first calculate the transmitted power through each slit. For this purpose, we excite the structure with a normally incident monochromatic plane wave (the green line in Fig. 1) having the transverse magnetic (TM) polarization, which has only the E_x, E_y, and H_z field components in the coordinate system we use. We calculate the transmitted power through each slit on a line patch very close to the exit surface of the slit. The width of the line patch is chosen in such a way that the power flux through it measures the transmitted power through an individual slit. The individual transmission cross section of each slit is then obtained by normalizing the individual transmitted power of each slit with respect to the incident power flux density. To calculate the overall transmission cross section of the entire structure, we calculate the transmitted power through all the three slits on a single connected line patch that covers all the exit surfaces of the slits, and normalize this power with respect to the incident power flux density.

Figure 2 shows the transmission cross section spectra for the lossy and lossless silver cases. The overall transmission cross section spectra in Fig. 2(d) show clear resonant behavior at the three different wavelengths, i.e., at 3411 nm, 4182 nm, and 4870 nm. The individual transmission cross section spectra in Figs. 2(a)–2(c) identify these resonances as belonging to the first, second, and third slit, respectively. The resonances are the result of the Fabry-Pérot-like behavior of the cavity modes supported by the deep-subwavelength slits for TM polarization.[9] The peak wavelengths of the transmission cross section resonances depend directly on the heights of individual slits. Indeed, we find that the resonance wavelength ratio is approximately equal to the height ratio of the slits, with a small redshift in the resonance wavelength due to the coupling to free-space modes.[21]

The transmission cross section of each 30-nm slit is on the order of micrometers at its resonance wavelength. For lossless silver, the peak transmission cross section for each resonance is very close to the maximal theoretical transmission cross section for an individual deep-subwavelength slit, which is λ/π.[20] For lossy silver, the peak is reduced somewhat, but the resonant behavior clearly persists. For example, when the slits are on resonance, the transmission cross sections in lossy metal case are 0.679 μm, 0.731 μm, and 0.790 μm for the first, second, and third slit, respectively. These values are more than 20 times the physical width of the slits (30 nm). Thus, while losses in the metal reduce the transmission cross sections, the peak transmission cross sections remain much larger than the physical size of the slits, and the transmission cross section resonances remain well separated in the frequency domain. Hence, spectral funneling, selection, and collection of light can be achieved with this device for realistic metal properties.

Even though the slits are physically very close to each other, i.e., at distances much smaller than their peak transmission cross sections and operating wavelengths, light of different wavelengths is funneled effectively to different slits (depending on its resonance wavelength). The transmission cross section for each slit is very small for all of its off-resonance wavelengths (particularly at the resonance wavelengths of other slits). Hence, the transmission cross section spectra shown in Fig. 2 exhibit negligible spectral crosstalk. This behavior is quite different from earlier reports on closely spaced arrays of nanoantennas with anti-Hermitian coupling, which shows selective excitation of individual antennas but with much larger interference effects.[7] As a further evidence of the lack of spectral crosstalk in this structure, Fig. 3 shows the magnetic field amplitude distribution ($|H_z|$) of the structure at the resonance wavelength of each slit. In each case, the field is concentrated in just one slit. Thus, light is funneled to only one slit at each resonance wavelength.

It has been shown that a single deep-subwavelength slit has a response that is independent of the angle of incidence.[20] As we show here, bringing such slits together does not introduce significant interaction between them. Therefore, the response of our spectral light separator should not depend on the angle of incidence either. In addition, the effect of spectral light separation occurs for light incident both from the top and the bottom of the thin metal film since it arises from the slit resonances, which can be excited from both sides. We also note that in this spectral light separator design, while the maximum field strength is at the interior of the resonant slits, there is still significant field strength at the exits of the resonant slits. Moreover, by placing the structure on a high-index substrate, the fields can be concentrated at the exit.[22]

In general, by tuning the geometrical properties of the apertures, we can control their resonance behavior. For the structure shown in Fig. 1, the width and height of each slit control its resonance behavior. For example, we have observed that an increase in the width decreases the quality factor of the resonance, whereas an increase in the height causes a redshift in the resonance wavelength. One can also change the resonance properties by adding a dielectric inside

or outside the slits. These procedures lead to a series of very straightforward design rules for this subwavelength spectral light separator.

As a side note, the individual transmission cross section spectra exhibit regions of negative transmission (Figs. 2(a)–2(c)). Near the resonance wavelength of each slit, there is negative power flow in the other slits that are off-resonance. This phenomenon is reminiscent of previously reported observations of negative power flow in periodic arrays of compound apertures.[23] However, our work here differs in that we consider aperiodic structures.

In an ideal multispectral imaging system, all spectrally selective detectors within a pixel should collect light from the same area of a scene in order to determine the spectral components (hence the "color") of that area. If this is not the case, spatial coregistration errors between different spectral channels can occur.[13] We illustrate this concept in Figs. 4(a) and 4(b). In Fig. 4(a), each of the three detectors (squares with differently colored outlines) detects a different spectral band, but gets its light from a different area in the scene (represented by the sequence of black and white regions at the top). In this case, the spectral components (hence the "color") of the white middle region of the scene are not fully captured by the imaging system. In contrast, Fig. 4(b) represents the ideal case, where each of the three spectrally selective detectors collects light from the same physical area; therefore, all the spectral components of the white middle region of the scene are detected, resulting in the full capture of the spectral information of that region by the imaging system.

We now illustrate that our design approaches the ideal case of Fig. 4(b), i.e., the slits in our subwavelength spectral light separator funnel and collect light from essentially the same physical area. For this purpose, we illuminate the structure with a top-hat monochromatic wave source with a spatial width of 1 μm. In our first set of calculations, we choose the frequency of the source to correspond to the resonance wavelength of the first slit. We shift the source horizontally (in the x-direction) and plot the power captured in the first slit as a function of source position as the blue curve in Fig. 4(c). Here, the power is normalized against the maximum captured power. We call this the spatial response. The
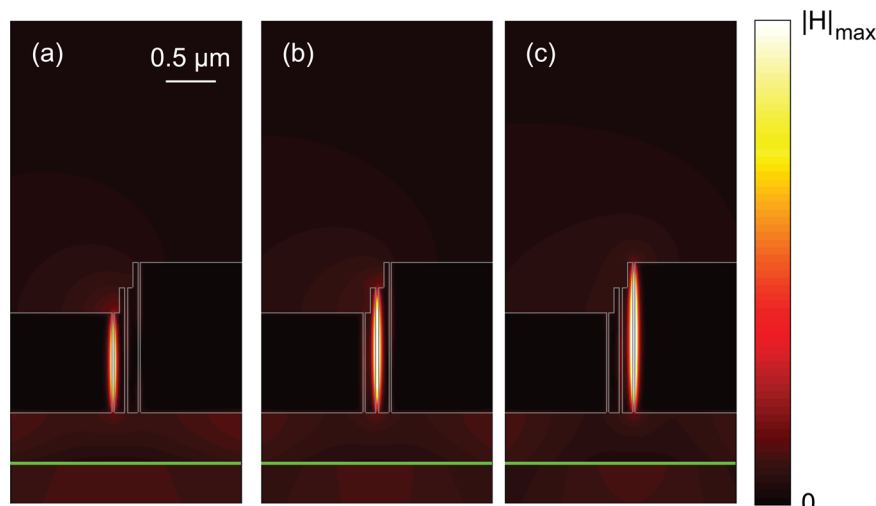
FIG. 3. Magnetic field amplitude distributions of the subwavelength spectral light separator excited at the resonance wavelength of each slit. (a)–(c) show the field amplitude distributions at $\lambda = 3411$ nm, $\lambda = 4182$ nm, and $\lambda = 4870$ nm, corresponding to the resonance wavelength of the first, second, and third slit, respectively.
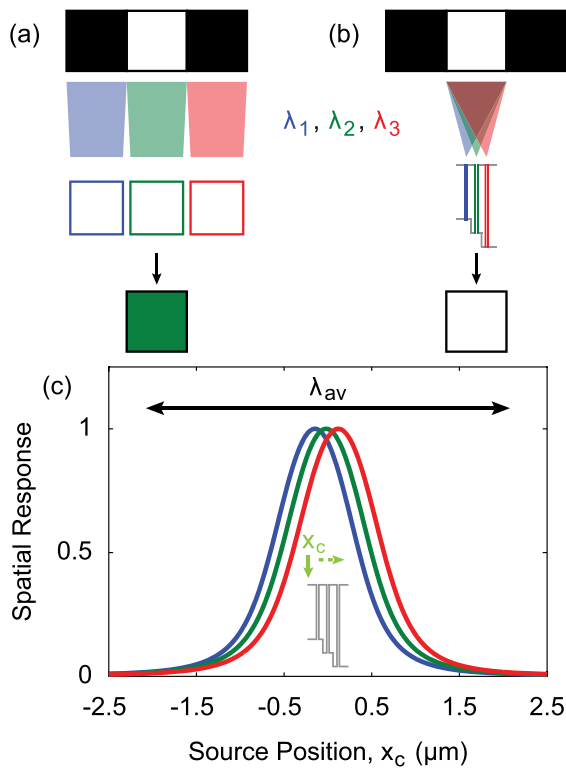
FIG. 4. Spatial response of the subwavelength spectral light separator. (a) A multispectral imaging system with spatial coregistration errors between three spectral channels (λ_1, λ_2, and λ_3). (b) A system based on our subwavelength spectral light separator eliminates spatial coregistration errors. (c) Spatial response of the subwavelength spectral light separator. The blue, green, and red lines correspond to the response of the first, second, and third slit at their respective resonance frequencies. x_c shows the position of the 1-μm-wide top-hat source, which is shifted to calculate the spatial response. λ_{av} is the average of the three resonance wavelengths.

spatial region where significant power is captured in the first slit defines the physical area from which the slit is capturing power. We repeat the same procedure above to compute the physical areas from which the second and third slits capture power (green and red curves in Fig. 4(c)). The average of the three resonance wavelengths λ_{av} is also drawn to scale in Fig. 4(c) for comparison.

Figure 4(c) shows that each slit captures power from an area that is centered at the slit, and this area has a width comparable to the transmission cross section of the slit. Since the spacing between the slits is at the deep-subwavelength scale, and the transmission cross sections are much larger than the slit widths, we see that the areas from which the slits capture power significantly overlap. In other words, each slit collects photons of a particular frequency from virtually the same broadband source area whose width is comparable to the wavelength size. As a result, our device eliminates spatial coregistration errors between spectral bands in multispectral imaging.

In summary, we have shown that a sequence of deep-subwavelength apertures in a metallic film can be designed to decompose light into its spectral components while being subwavelength in size and at the same time extremely photon-efficient, which is of great importance in multispectral imaging applications. As a specific example of such a subwavelength spectral light separator, we have designed a metallic structure with three deep-subwavelength slits and calculated the individual and overall transmission cross section spectra to show resonances in transmission. To demonstrate the feasibility of the structure, we compared the performance of the structure made of lossless metal with that of lossy metal. We have also shown that the electromagnetic field is concentrated in only one slit at that slit's resonance wavelength. Finally, we have demonstrated that different slits capture light coming from the same area, which eliminates spatial coregistration errors in multispectral imaging. The size of the entire structure is at the subwavelength scale. Thus, this device can be used to create much more compact filtering devices, thanks to the unique properties of deep-subwavelength apertures.

[1]X. Prieto-Blanco, C. Montero-Orille, B. Couce, and R. de la Fuente, in *Computational Intelligence for Remote Sensing*, edited by M. Graña and R. J. Duro (Springer, Berlin, Heidelberg, 2008), Chap. 1.
[2]G. Themelis, J. S. Yoo, and V. Ntziachristos, Opt. Lett. **33**, 1023 (2008).
[3]Y. Garini, I. T. Young, and G. McNamara, Cytometry, Part A **69A**, 735 (2006).
[4]N. Tack, A. Lambrechts, P. Soussan, and L. Haspeslagh, Proc. SPIE **8266**, 82660Q (2012).
[5]E. Laux, C. Genet, T. Skauli, and T. W. Ebbesen, Nat. Photonics **2**, 161 (2008).
[6]J. L. Perchec, Y. Desieres, N. Rochat, and R. E. de Lamaestre, Appl. Phys. Lett. **100**, 113305 (2012).
[7]S. Zhang, Z. Ye, Y. Wang, Y. Park, G. Bartal, M. Mrejen, X. Yin, and X. Zhang, Phys. Rev. Lett. **109**, 193902 (2012).
[8]J. A. Porto, F. J. García-Vidal, and J. B. Pendry, Phys. Rev. Lett. **83**, 2845 (1999).
[9]Y. Takakura, Phys. Rev. Lett. **86**, 5601 (2001).
[10]S.-H. Chang, S. Gray, and G. Schatz, Opt. Express **13**, 3150 (2005).
[11]A. Degiron, H. J. Lezec, N. Yamamoto, and T. W. Ebbesen, Opt. Commun. **239**, 61 (2004).
[12]Z. Ruan and M. Qiu, Phys. Rev. Lett. **96**, 233901 (2006).
[13]T. Skauli, Opt. Express **20**, 918 (2012).
[14]E. D. Palik, *Handbook of Optical Constants of Solids* (Academic Press, 1985).
[15]N. J. Champagne II, J. G. Berryman, and H. M. Buettner, J. Comput. Phys. **170**, 830 (2001).
[16]G. Veronis and S. Fan, in *Surface Plasmon Nanophotonics*, edited by M. L. Brongersma and P. G. Kik (Springer, Netherlands, 2007), Chap. 12.
[17]U. S. Inan and R. A. Marshall, in *Numerical Electromagnetics: The FDTD Method* (Cambridge University Press, 2011), Chap. 14.
[18]W. Shin and S. Fan, Opt. Express **21**, 22578 (2013).
[19]W. Shin and S. Fan, J. Comput. Phys. **231**, 3406 (2012).
[20]L. Verslegers, Z. Yu, P. B. Catrysse, and S. Fan, J. Opt. Soc. Am. B **27**, 1947 (2010).
[21]F. J. Garcia-Vidal, L. Martin-Moreno, T. W. Ebbesen, and L. Kuipers, Rev. Mod. Phys. **82**, 729 (2010).
[22]J. S. White, G. Veronis, Z. Yu, E. S. Barnard, A. Chandran, S. Fan, and M. L. Brongersma, Opt. Lett. **34**, 686 (2009).
[23]A. Enemuo, M. Nolan, Y. U. Jung, A. B. Golovin, and D. T. Crouse, J. Appl. Phys. **113**, 014907 (2013).